Calculation of the convex roof for an open entangled harmonic oscillator system

Mayer A. Landau* and C. R. Stroud, Jr.
The Institute of Optics, University of Rochester, Rochester, New York 14627, USA
(Received 9 October 2009; published 6 May 2010)

We explicitly calculate the time dependence of entanglement via the convex roof extension for a system of noninteracting harmonic oscillators. These oscillators interact only indirectly with each other by way of a zero-temperature bath. The initial state of the oscillators is taken to be that of an entangled Schrödinger-cat state. This type of initial condition leads to superexponential decay of the entanglement when the initial state has the same symmetry as the interaction Hamiltonian.

DOI: 10.1103/PhysRevA.81.052304 PACS number(s): 03.67.Mn, 03.65.Ud

I. INTRODUCTION

Two central issues in the field of quantum entanglement concern quantifying the degree of entanglement in an open system and protecting the system's entanglement from the external environment. Quantifying entanglement is important in devising potential applications for entanglement. Protecting entanglement is essential for actualization of entanglement as a resource.

In protecting entanglement, mathematically at least, there is a satisfying beginning, namely, starting with a Hamiltonian that possesses some type of symmetry [1–4]. Then the Hilbert space will split into a decohering part and a decoherence-free part. The decohering part will contain initial states that possess the symmetry of the Hamiltonian, and the decoherence-free part will contain initial states that do not possess this symmetry. Experimentally, such decoherence-free subspaces have been realized [5–7].

In quantifying entanglement the mathematical situation is less satisfying. Entanglement for pure states in the bipartite case is adequately described by the entropy [8,9]. For bipartite mixed states the situation is settled for qubits with Wootters' concurrence [10,11]. As the partition number and level structure of the system increases there become increasingly many (in fact exponentially so) different types of entanglement under local unitary operations [12–17]. The number of proposed entanglement measures has likewise proliferated [18–23]. For mixed states there is an added complication. Even after one settles on an appropriate measure of entanglement for pure states, mixed states require the application of the convex roof extension.

The convex roof entails a decomposition of the density matrix into pure states. Each possible decomposition is in a one-to-one correspondence with some unitary matrix [24]. The convex roof thus relies on searching the Lie group SU(K) for the decomposition that gives minimal entanglement. Here, K can theoretically be as large as the square of the rank of the density matrix [25]. For example, for a three-level tripartite system the density matrix could have rank as high as 27. Then, we might have to search a Lie group as large as SU(27^2), which has a dimension of $27^4 - 1$. Thus, in the general case it is numerically impractical to compute the convex roof. This has led to a great number of articles that give analytical estimates for the convex roof [26–31], but where actual calculation is limited to the two-level bipartite case or in the tripartite case to rank 2, 3, or 4 density matrices for a two-level system [32–34] with special mixtures. All these sources deal with discrete systems. In this article we perform a convex roof calculation for a tripartite three-level continuous variable system.

It turns out that the well-studied model [35–40] of a system of harmonic oscillators prepared initially in a Schrödinger cat state and interacting only via a zero-temperature bath can have the convex roof extension evaluated by a modest numerical calculation. This is a nice model to study because its time dependence can be solved explicitly and the Hamiltonian has well-defined symmetry. The Hilbert space thus separates into decohering and decoherence-free subspaces. At first sight, it seems the convex roof in such a model would be quite difficult to calculate because in this case we are dealing with continuous variable entanglement. However, by utilizing the symmetry of the Hamiltonian in the choice of initial state, one can reduce the continuous system to one with effectively a finite number of levels [41]. Under such a change of basis, the convex roof is in fact numerically computable with modest resources. This happens because the rank of the density matrix is much smaller than the maximally possible value. This means that the range of Lie groups one has to search starts at a much lower dimension. Furthermore, numerical results strongly suggest that the convex roof is attained at the minimum of this range of Lie groups for this particular model. This suggests that while the calculation of the convex roof appears quite formidable in theory, in practice for many systems, numerically computing the convex roof is not terribly difficult.

Our model, in full generality, has an arbitrary number of levels and parties. In calculating the convex roof, we chose as our measure for pure states the entanglement monotone of Barnum, Knill, Ortiz, and Viola [42–46], which we abbreviate as BKOV. We do not claim that this measure is more or less appropriate than any other measure. It is known that it cannot distinguish the product of two Bell states from a four-party Greenberger-Horne-Zeilinger (GHZ) state [47]. These product-entangled states do not occur in our model. Because of the symmetry of our interaction Hamiltonian and our initial conditions, we sample only a particular set of states in going from initial to final states. We are not concerned about the entanglement of states we do not sample. Therefore, BKOV, because it is the only measure to our knowledge that can be applied to systems with no level or party number restriction, seems appropriate. It gives reasonable results for

*landau@optics.rochester.edu

our model. However, we point out that the particular measure is unimportant for this proof of principle. One chooses the measure one feels is most appropriate and then proceeds to calculate its convex roof.

In what follows, we present our version of the previously described model. We find the time dependence of the system and bath operators in the Markov approximation. Next, we determine the decohering and decohrence-free subspaces of the Hilbert space. After tracing out the bath, we transform the system to a new basis that gives us a finite dimensional Hilbert space. Finally, we numerically calculate the convex roof for the system oscillators when the initial state is a Schrödinger cat in a decohering subspace of the overall Hilbert space.

II. MODEL HAMILTONIAN

Consider a set of N oscillators, which we will call the system oscillators in what follows. We will assume that these system oscillators do not interact directly with each other, but rather indirectly via a reservoir of a countably infinite set of bath oscillators. The system Hamiltonian is then given by

$$\mathbf{H} = \sum_{p=0}^{N-1} \hbar\omega \hat{a}_p^\dagger \hat{a}_p + \sum_{B=0}^{\infty} \hbar\omega_B \hat{b}_B^\dagger \hat{b}_B + \sum_{B=0}^{\infty} \kappa_B \left(\hat{b}_B^\dagger \sum_{p=0}^{N-1} \hat{a}_p + \text{H.c.} \right), \tag{1}$$

where κ_B denotes a different coupling constant between each bath oscillator and the system oscillators. We also assume symmetric coupling of the system oscillators to the bath. In the case in which the reservoir is the electromagnetic field, this is the Dicke long wavelength limit. With this coupling scheme, the system evolves into nonsymmetric states (see [48] for details). For this model we can assume that some or all of the system oscillators are initially excited, while the bath oscillators are all initially in their ground state. This situation is illustrated by the following initial state:

$$|\Psi(0)\rangle = \mathcal{N} \sum_{\sigma=0}^{M-1} |\psi_\sigma\rangle, \tag{2}$$

where

$$|\psi_\sigma(0)\rangle = \left[\bigotimes_{p=0}^{N-1} |\alpha_{\sigma,p}(0)\rangle \right] \otimes \left[\bigotimes_{B} |\beta_{\sigma,B}(0)\rangle \right]. \tag{3}$$

Here $|\alpha_{\sigma,p}(0)\rangle$ and $|\beta_{\sigma,B}(0)\rangle$ are coherent states, including the possibility of the vacuum state.

Notice that $|\Psi(0)\rangle$ is a continuous variable multipartite entangled Schrödinger-cat state provided $M \geqslant 1$. This is because each party is a superposition of M different coherent states. Being in a superposition of coherent states, that is, a Schrödinger-cat state, is necessary for the entanglement. Furthermore, if we trace out the bath oscillators, then we see that the initial system state is the pure entangled Schrödinger-cat state,

$$|\Psi(0)\rangle = \mathcal{N} \sum_{\sigma=0}^{M-1} \left[\bigotimes_{p=0}^{N-1} |\alpha_{\sigma,p}(0)\rangle \right]. \tag{4}$$

For large α this state approaches a GHZ state, and so in that sense the entanglement is maximal. We wish to explore the decay of this entanglement with time

The time dependence of this state can be found by solving the Heisenberg equations of motion for the time dependence of the operators $\hat{a}_{\sigma,p}(t)$ and $\hat{b}_{\sigma,B}(t)$. This is most easily done by performing the change of variables,

$$\hat{A}_p = \frac{1}{\sqrt{N}} \sum_{q=0}^{N-1} \hat{a}_q e^{2\pi i p q/N}, \tag{5}$$

for $0 \leqslant p \leqslant N-1$. The Heisenberg equations of motion now take the form

$$\dot{\hat{A}}_p = -i\omega \hat{A}_p - i\delta_{p,0}\sqrt{N} \sum_B \kappa_B \hat{b}_B, \tag{6}$$

$$\dot{\hat{b}}_B = -i\omega_B \hat{b}_B - i\sqrt{N}\kappa_B \hat{A}_0. \tag{7}$$

In making this change of variables, we have used the symmetry of the coupling between each system oscillator and the bath.

We can immediately solve Eq. (6) for the case $p > 0$ to get

$$\hat{A}_p(t) = \hat{A}_p(0) e^{-i\omega t}, \quad p > 0 \tag{8}$$

and formally integrate Eq. (7) to get

$$\hat{b}_B(t) = \hat{b}_B(0) e^{-i\omega_B t} - i\sqrt{N}\kappa_B \int_0^t dt' e^{-i\omega_B (t-t')} \hat{A}_0(t'). \tag{9}$$

Substituting Eq. (9) into Eq. (6) we get

$$\dot{\hat{A}}_0(t) = -i\omega \hat{A}_0 - i\sqrt{N} \sum_B \kappa_B \hat{b}_B(0) e^{-i\omega_B t} - N \sum_B \kappa_B^2 \int_0^t dt' e^{-i\omega_B (t-t')} \hat{A}_0(t'). \tag{10}$$

Next, we allow our bath modes to become a continuum introducing an appropriate density of states:

$$\dot{\hat{A}}_0(t) = -i\omega \hat{A}_0 - i\sqrt{N} \sum_B \kappa_B \hat{b}_B(0) e^{-i\omega_B t} - N \int_0^\infty d\omega_B \varrho(\omega_B) \kappa^2(\omega_B) \int_0^t dt' e^{-i\omega_B (t-t')} \hat{A}_0(t'). \tag{11}$$

Applying the standard Markov approximation argument [49], and ignoring the Lamb shift, we arrive at our final equation:

$$\dot{\hat{A}}_0(t) = -i\omega \hat{A}_0 - i\sqrt{N} \sum_B \kappa_B \hat{b}_B(0) e^{-i\omega_B t} - \pi N \hat{A}_0(t) \varrho(\omega) \kappa^2(\omega). \tag{12}$$

This equation can be easily integrated to get

$$\hat{A}_0(t) = \hat{A}_0(0) e^{-(i\omega + N\gamma)t} - i\sqrt{N} \sum_B \kappa_B \hat{b}_B(0) \times \frac{e^{-i\omega_B t} - e^{-(i\omega + N\gamma)t}}{i(\omega - \omega_B) + N\gamma}, \tag{13}$$

where $\gamma = \pi \varrho(\omega) \kappa^2(\omega)$ is the reservoir damping constant for a single oscillator.

We can now transform back to the $\hat{a}_p$ variables using the inverse transform

$$\hat{a}_p = \frac{1}{\sqrt{N}} \sum_{q=0}^{N-1} \hat{A}_q e^{-2\pi i p q/N}. \tag{14}$$

As the bath oscillators are initially in their ground state, we can discard terms of the form $\hat{b}_B(0)$ in our expression for $\hat{a}(t)$ and $\hat{b}(t)$. The result is

$$\hat{a}_p(t) = \hat{a}_p(0) e^{-i\omega t} + \frac{e^{-i\omega t}}{N}(e^{-N\gamma t} - 1) \sum_{q=0}^{N-1} \hat{a}_q(0), \tag{15}$$

and

$$\hat{b}_B(t) = \kappa_B \left[\frac{1}{\sqrt{N}} \sum_{p=0}^{N-1} \hat{a}_p(0) \right] \frac{e^{-(i\omega + N\gamma)t} - e^{-i\omega_B t}}{(\omega - \omega_B) - iN\gamma}. \tag{16}$$

We note that if

$$\hat{a}(t)|\alpha(0)\rangle = \alpha(t)|\alpha(0)\rangle \tag{17}$$

in the Heisenberg picture, then

$$\hat{a}(0)|\alpha(t)\rangle = \alpha(t)|\alpha(t)\rangle \tag{18}$$

in the Schrödinger picture.

Applying $\hat{a}(t)$ and $\hat{b}(t)$ to the initial state [Eq. (3)], we get

$$\begin{aligned} &\hat{a}_p(t)|\psi_\sigma(0)\rangle \\ &\quad = e^{-i\omega t} \left[\alpha_{\sigma,p}(0) + \frac{1}{N}(e^{-N\gamma t} - 1) \sum_{q=0}^{N-1} \alpha_{\sigma,q}(0) \right] |\psi_\sigma(0)\rangle \\ &\quad \equiv \alpha_{\sigma,p}(t)|\psi_\sigma(0)\rangle \end{aligned} \tag{19}$$

and

$$\begin{aligned} &\hat{b}_B(t)|\psi_\sigma(0)\rangle \\ &\quad = \kappa_B \frac{1}{\sqrt{N}} \left[\sum_{p=0}^{N-1} \alpha_{\sigma,p}(0) \right] \frac{e^{-(i\omega + N\gamma)t} - e^{-i\omega_B t}}{(\omega - \omega_B) - iN\gamma} |\psi_\sigma(0)\rangle \\ &\quad \equiv \beta_{\sigma,B}(t)|\psi_\sigma(0)\rangle, \end{aligned} \tag{20}$$

respectively. So $|\psi_\sigma(0)\rangle$ satisfies the conditions of Eq. (17). Knowing its time dependence of course gives us the time dependence of the full wave function in Eq. (2). Thus,

$$|\psi_\sigma(t)\rangle = \left[\bigotimes_{p=0}^{N-1} |\alpha_{\sigma,p}(t)\rangle \right] \otimes \left[\bigotimes_{B} |\beta_{\sigma,B}(t)\rangle \right]. \tag{21}$$

and

$$|\Psi(t)\rangle = \mathcal{N} \sum_{\sigma=0}^{M-1} |\psi_\sigma(t)\rangle. \tag{22}$$

III. INITIAL CONDITIONS

Consider the case in which we have N system oscillators and P of these are initially excited. When an oscillator is excited, we take it to be in a generalized Schrödinger-cat superposition that is symmetric in phase around the phase-space orbit [41]. We then have

$$|\alpha_{\sigma,p}(0)\rangle = \begin{cases} |\mu e^{2\pi i\sigma/M}\rangle & \text{when } p = 0, \\ |\mu e^{2\pi i\sigma/M + i\theta_p}\rangle & \text{when } 1 \leqslant p < P, \\ |0\rangle & \text{otherwise,} \end{cases} \tag{23}$$

where the θ_p are arbitrary angles for now. From Eq. (19) the resulting α eigenvalues for the system oscillators are now

$$\alpha_{\sigma,p}(t) = \begin{cases} \Delta \left[1 + (e^{-N\gamma t} - 1) \frac{\left(1 + \sum_{q=1}^{P-1} e^{i\theta_q}\right)}{N} \right], \\ p = 0, \\ \Delta \left[e^{i\theta_p} + (e^{-N\gamma t} - 1) \frac{\left(1 + \sum_{q=1}^{P-1} e^{i\theta_q}\right)}{N} \right], \\ 1 \leqslant p < P, \\ \Delta (e^{-N\gamma t} - 1) \frac{\left(1 + \sum_{q=1}^{P-1} e^{i\theta_q}\right)}{N}, \\ p \geqslant P, \end{cases} \tag{24}$$

where

$$\Delta = e^{-i\omega t} \mu e^{2\pi i\sigma/M}. \tag{25}$$

There is a special initial state that is decoupled from the bath and for that we must have

$$1 + \sum_{q=1}^{P-1} e^{i\theta_q} = 0, \tag{26}$$

which implies that the bath eigenvalues remain zero as well. The preceding condition is satisfied, for example, when $\theta_q = 2\pi Sq/P$ for integer S with $S \neq 0$. Different integer values of S mod P define orthogonal decoherence-free subspaces of the Hilbert space. In this case the given symmetry decouples the system oscillators from the bath, and there is no decay of the original pure state.

It is not hard to see as well that for maximal decoherence we must have $P = N$ and

$$1 + \sum_{q=1}^{N-1} e^{i\theta_q} = N. \tag{27}$$

This requires that $e^{i\theta_q} = 1$. That is, all the oscillators are in the same state, and we have the case of superradiance with maximal cooperativity [50]. The amplitudes of the $\alpha_{\sigma,p}(t)$ take the form

$$\alpha_{\sigma,p}(t) = \mu e^{-i\omega t} e^{2\pi i\sigma/M} e^{-N\gamma t}; \tag{28}$$

that is, the system oscillator amplitudes decay away completely as $t \to \infty$.

IV. REDUCED DENSITY MATRIX

We are interested in the time evolution of the entanglement of the system oscillators in the superradiant case. As a first

step we compute the reduced density matrix as a function of time. Tracing over the bath, the reduced density matrix for the system oscillators is given by

$$\hat{\rho}_S = \mathcal{N}^2 \sum_{\sigma,\varsigma=0}^{M-1} \bigotimes_{p=0}^{N-1} |\alpha_{\sigma,p}\rangle\langle\alpha_{\varsigma,p}| \prod_B \langle\beta_{\varsigma,B}|\beta_{\sigma,B}\rangle, \tag{29}$$

with normalization $\mathcal{N}^2$ calculated from the unit trace condition

$$1 = \mathcal{N}^2 \sum_{\sigma,\varsigma=0}^{M-1} \prod_{p=0} \langle\alpha_{\sigma,p}|\alpha_{\varsigma,p}\rangle \prod_B \langle\beta_{\sigma,B}|\beta_{\varsigma,B}\rangle. \tag{30}$$

Now,

$$\begin{aligned}\prod_B &\langle\beta_{\sigma,B}|\beta_{\varsigma,B}\rangle \\ &= \prod_B \exp\{-N|\bar{\mu}|^2[1-e^{-2\pi i(\sigma-\varsigma)/M}]|f_B(t)|^2\} \\ &= \exp\left\{-N|\bar{\mu}|^2[1-e^{-2\pi i(\sigma-\varsigma)/M}]\sum_B |f_B(t)|^2\right\},\end{aligned} \tag{31}$$

where

$$\bar{\mu} \equiv \frac{\left(1+\sum_{q=1}^{P-1} e^{i\theta_q}\right)}{N}\mu \tag{32}$$

and

$$\begin{aligned}|f_B(t)|^2 &= |\kappa_B|^2 \left\{\frac{e^{-2N\gamma t} - 2e^{-N\gamma t}\cos[(\omega-\omega_B)t]+1}{(\omega-\omega_B)^2+N^2\gamma^2}\right\} \\ &\equiv |\kappa_B|^2 \mathcal{F}_B.\end{aligned} \tag{33}$$

We can approximate the sum over all f_B as follows:

$$\begin{aligned}\sum_B |f_B(t)|^2 &= \int_{-\infty}^{\infty} \varrho(\omega_B)|f_B(\omega_B,t)|^2 d\omega_B \\ &\approx \varrho(\omega)|\kappa(\omega)|^2 \int_{-\infty}^{\infty} \mathcal{F}_B d\omega_B \\ &= \frac{\pi}{N\gamma}\varrho(\omega)|\kappa(\omega)|^2(1-e^{-2N\gamma t}).\end{aligned} \tag{34}$$

Using our definition of γ, we find

$$\sum_B |f_B(t)|^2 = \frac{1}{N}(1-e^{-2N\gamma t}). \tag{35}$$

Finally, we have

$$\prod_B \langle\beta_{\sigma,B}|\beta_{\varsigma,B}\rangle = \exp\{-|\bar{\mu}|^2[1-e^{-2\pi i(\sigma-\varsigma)/M}](1-e^{-2N\gamma t})\}. \tag{36}$$

Of special importance in this equation for what follows will be the off-diagonal bath inner-product (ODBIP) terms, that is, those for which $\sigma \neq \varsigma$. This is because the degree of coherence between the system terms depends on the amount of overlap of the different bath terms [51].

We can check that Eq. (36) holds at $t = 0$,

$$\prod_B \langle\beta_{\sigma,B}|\beta_{\varsigma,B}\rangle = 1, \tag{37}$$

and that

$$\begin{aligned}\hat{\rho}_S(0) &= \mathcal{N}^2 \sum_{\sigma,\varsigma=0}^{M-1} \bigotimes_{p}^{N-1} |\alpha_{\sigma,p}\rangle\langle\alpha_{\varsigma,p}| \\ &= \left(\mathcal{N}\sum_{\sigma=0}^{M-1}\bigotimes_{p}^{N-1}|\alpha_{\sigma,p}\rangle\right)\left(\mathcal{N}\sum_{\varsigma=0}^{M-1}\bigotimes_{q}^{N-1}\langle\alpha_{\varsigma,q}|\right);\end{aligned} \tag{38}$$

that is, the state is pure at time $t = 0$.

From

$$\begin{aligned}\prod_{p=0}^{N-1}\langle\alpha_{\sigma,p}|\alpha_{\varsigma,p}\rangle &= \exp\{-|\bar{\mu}|^2 e^{-2N\gamma t}[1-e^{-2\pi i(\sigma-\varsigma)/M}]\}^N \\ &= \exp\{-N|\bar{\mu}|^2 e^{-2N\gamma t}[1-e^{-2\pi i(\sigma-\varsigma)/M}]\},\end{aligned} \tag{39}$$

we have that the normalization $\mathcal{N}^2$ is given by

$$\begin{aligned}\frac{1}{\mathcal{N}^2} &= \frac{\mathrm{tr}\{\hat{\rho}_S(t)\}}{\mathcal{N}^2} \\ &= \sum_{\sigma,\varsigma=0}^{M-1} \exp\{-[1+(N-1)e^{-2N\gamma t}]|\bar{\mu}|^2 \\ &\quad\times[1-e^{-2\pi i(\sigma-\varsigma)/M}]\}.\end{aligned} \tag{40}$$

When $|\bar{\mu}| \gtrsim 2$, the real part of the ODBIP terms decay extremely rapidly from 1 to e^{-1} in the period

$$0 \leqslant t \leqslant \frac{-1}{2N\gamma}\log_e\left(1-\frac{1}{|\bar{\mu}|^2}\right).$$

This is due to the $\exp[1-\exp(-2N\gamma t)]$ dependence on t in the exponent of Eq. (36). The final factor,

$$G = \exp\{-|\bar{\mu}|^2[1-\cos(2\pi i(\sigma-\varsigma)/M)]\} \equiv e^{-g},$$

is more than an order of magnitude smaller than one. Practically, this gives a superexponential decay rate for the coherence. We call this superexponential because

$$\mathrm{Re}\left\{\prod_B \langle\beta_{\sigma,B}|\beta_{\varsigma,B}\rangle\right\} = e^{-g}\exp(ge^{-2N\gamma t}). \tag{41}$$

For small t and large g this decay rate is much faster than the $\exp(-N\gamma t)$ decay rate for the system oscillator amplitudes.

During this period the reduced density matrix decays to

$$\hat{\rho}_S(t) = \mathcal{N}^2 \sum_{\sigma=0}^{M-1}\bigotimes_{p=0}^{N-1}|\alpha_{\sigma,p}(t)\rangle\langle\alpha_{\sigma,p}(t)|. \tag{42}$$

This density matrix is mixed.

The system amplitude undergoes decay at the slower exponential rate. In the situation of Eq. (27), where all the oscillators are initially excited with the same phase, all the system oscillators reduce to the ground state in a time $t \gtrsim \frac{1}{N\gamma}$ and the quantum state of the system becomes pure again. In this case, we see that in Eq. (40) the dominant terms in the sum are the ones where $\varsigma = \sigma$. There are M such terms, so that

$$\frac{1}{\mathcal{N}^2} \sim M. \tag{43}$$

V. A BASIS AND MEASURE FOR EVALUATING ENTANGLEMENT

The state of the system in each party is specified by M coherent states that depend on time as given by Eq. (28). To evaluate the entanglement of the system, an orthonormal basis for these coherent states is required. We form a minimal dynamic orthonormal basis, that is, a basis that evolves with time, by transforming from the $|\alpha_{\sigma,p}\rangle$ basis to the orthonormal $|V_{\sigma,p}\rangle$ basis given in [41]. From [41, Eq. (22)] we have

$$|\alpha_{\sigma,p}\rangle = \frac{1}{M}\sum_{\varsigma=0}^{M-1}\mathcal{N}_\varsigma \exp(2\pi i\sigma\varsigma/M)|V_{\varsigma,p}\rangle, \tag{44}$$

where the orthonormal $|V_{\varsigma,p}\rangle$ basis is given in [41], Eq. (23)] by

$$|V_{\varsigma,p}\rangle = \frac{1}{\mathcal{N}_\varsigma}\sum_{\sigma=0}^{M-1}\exp(-2\pi i\sigma\varsigma/M)|\lambda_p(t)e^{2\pi i\sigma/M}\rangle, \tag{45}$$

and the normalization factors $\mathcal{N}_\sigma$ are given by

$$\mathcal{N}_\sigma^2 = M\sum_{\varsigma=0}^{M-1}[(e^{-2\pi i\varsigma/M})^\sigma \exp\{|\lambda_p(t)|^2[\exp(2\pi i\varsigma/M)-1]\}]. \tag{46}$$

Transformation to this basis is possible by virtue of the symmetry we specified for our initial conditions. Because all coherent states decay in identical fashion, this symmetry is preserved for all time. This time-independent symmetry enables us to rewrite the state of the system, given by M independent coherent states in each party, in terms of an orthonormal basis with M elements for each party. The system is thus represented as a well defined M-level, N-partite system. This allows us to apply various discrete entanglement measures to our system. For example, for the superradiant case, when $t=0$, we see that we have a maximally entangled (in the GHZ sense) state. The BKOV measure [42,43] is defined for multipartite, multilevel systems and it sets the GHZ state as the maximally entangled state. So we analyze the entanglement using the BKOV measure. Since our reduced density matrices are mixed, we calculate the convex roof extension (CRE) of the BKOV measure.

VI. CONVEX ROOF CALCULATION

Calculating the CRE of a pure state entanglement measure requires writing the density matrix in the form

$$\hat{\rho} = \sum_\sigma p_\sigma |\Psi_\sigma\rangle\langle\Psi_\sigma|, \tag{47}$$

where $\sum p_\sigma = 1$ and the $|\Psi_\sigma\rangle$ represent pure states. This decomposition is not unique, and indeed is parametrized by the special unitary groups SU(K) [24]. In the case where the Ψ_σ are orthogonal, the p_σ are the eigenvalues of the density matrix, and the decomposition is called the eigendecomposition [52]. For a general density matrix, written with respect to an orthonormal basis, rewriting $\hat{\rho}$ in the form of Eq. (47) so that each term in the decomposition is orthogonal requires that we diagonalize the given density matrix. In the case where the density matrix $\hat{\rho}$ has degenerate eigenvalues, this implies that the diagonalizing matrix $\boldsymbol{D}$ is not unique. The number of positive eigenvalues of $\hat{\rho}$ is the rank.

Given an orthogonal decomposition of $\hat{\rho}$, we can evaluate the entanglement of this decomposition by taking the value

$$\sum_\sigma p_\sigma \times \text{entanglement}(|\Psi_\sigma\rangle); \tag{48}$$

that is, one evaluates the entanglement of each pure state $|\Psi_\sigma\rangle$ and multiplies by the weighting factor p_σ and then sums the terms. To calculate the entanglement of $\hat{\rho}$, one must repeat this step for all possible decompositions of $\hat{\rho}$, and take the minimum value. This means taking the value

$$\sum_\sigma q_\sigma \times \text{entanglement}(|\Phi_\sigma\rangle), \tag{49}$$

where

$$\begin{pmatrix}\sqrt{q_0}|\Phi_0\rangle\\ \vdots\\ \sqrt{q_{K-1}}|\Phi_{K-1}\rangle\end{pmatrix} = \boldsymbol{T}\begin{pmatrix}\sqrt{p_0}|\Psi_0\rangle\\ \vdots\\ \sqrt{p_{\text{rank}\{\hat{\rho}\}-1}}|\Psi_{\text{rank}\{\hat{\rho}\}-1}\rangle\\ 0_{\text{rank}\{\hat{\rho}\}}\\ \vdots\\ 0_{K-1}\end{pmatrix}. \tag{50}$$

Here $\sum_{\varsigma=0}^{K-1} q_\varsigma = 1$ and $\boldsymbol{T}$ is a $K \times \text{rank}\{\hat{\rho}\}$ size submatrix of a unitary matrix $\boldsymbol{U} \in \text{SU}(K)$.

We illustrate with an example. We consider the density matrix of the form

$$\hat{\rho} = \frac{1}{4}\begin{pmatrix}1&0&0&1\\0&1&1&0\\0&1&1&0\\1&0&0&1\end{pmatrix}, \tag{51}$$

given in the

$$|00\rangle, |01\rangle, |10\rangle, |11\rangle \tag{52}$$

basis. Since this matrix is bipartite two level, one could apply the concurrence to verify that $\hat{\rho}$ has zero entanglement. Instead, we will find the entanglement of $\hat{\rho}$ by taking the convex roof directly. The matrix that diagonalizes this density matrix is given by

$$\boldsymbol{D} = \frac{1}{\sqrt{2}}\begin{pmatrix}0&1&0&1\\1&0&1&0\\1&0&-1&0\\0&1&0&-1\end{pmatrix}, \tag{53}$$

so that

$$\hat{\rho} = \boldsymbol{D}\begin{pmatrix}\frac{1}{2}&0&0&0\\0&\frac{1}{2}&0&0\\0&0&0&0\\0&0&0&0\end{pmatrix}\boldsymbol{D}^\dagger \tag{54}$$

and the diagonal basis is given by

$$\begin{pmatrix} |\Psi_0\rangle \\ |\Psi_1\rangle \\ |\Psi_2\rangle \\ |\Psi_3\rangle \end{pmatrix} = \boldsymbol{D}^\dagger \begin{pmatrix} |00\rangle \\ |01\rangle \\ |10\rangle \\ |11\rangle \end{pmatrix}. \tag{55}$$

One way to write this, which is useful for the general case, is

$$|\Psi_\sigma\rangle = \sum_{m=0}^{3} D^\dagger_{\sigma m} |m\rangle, \tag{56}$$

where we have numbered the basis elements as

$$|0\rangle \equiv |00\rangle, \quad |1\rangle \equiv |01\rangle, \quad |2\rangle \equiv |10\rangle, \quad |3\rangle \equiv |11\rangle. \tag{57}$$

Our decomposition is of the form

$$\hat{\rho} = \tfrac{1}{2}|\Psi_0\rangle\langle\Psi_0| + \tfrac{1}{2}|\Psi_1\rangle\langle\Psi_1|, \tag{58}$$

where

$$\begin{aligned} |\Psi_0\rangle &= \sqrt{\tfrac{1}{2}}(|01\rangle + |10\rangle), \\ |\Psi_1\rangle &= \sqrt{\tfrac{1}{2}}(|00\rangle + |11\rangle). \end{aligned} \tag{59}$$

Obviously, both $|\Psi_0\rangle$ and $|\Psi_1\rangle$ are Bell states, so any entanglement measure on this decomposition will give full entanglement.

To do better, we try $\boldsymbol{T} = \boldsymbol{U} \in SU(2)$. Then we have

$$\hat{\rho} = q_0|\Phi_0\rangle\langle\Phi_0| + q_1|\Phi_1\rangle\langle\Phi_1|, \tag{60}$$

where

$$\begin{pmatrix} \sqrt{q_0}|\Phi_0\rangle \\ \sqrt{q_1}|\Phi_1\rangle \end{pmatrix} = \begin{pmatrix} U_{00} & U_{01} \\ U_{10} & U_{11} \end{pmatrix} \begin{pmatrix} \sqrt{p_0}|\Psi_0\rangle \\ \sqrt{p_1}|\Psi_1\rangle \end{pmatrix}. \tag{61}$$

Since $p_0 = \frac{1}{2} = p_1$, it is clear that we also have $q_0 = \frac{1}{2} = q_1$, so

$$\begin{pmatrix} |\Phi_0\rangle \\ |\Phi_1\rangle \end{pmatrix} = \begin{pmatrix} U_{00} & U_{01} \\ U_{10} & U_{11} \end{pmatrix} \begin{pmatrix} |\Psi_0\rangle \\ |\Psi_1\rangle \end{pmatrix}. \tag{62}$$

If we let

$$\boldsymbol{U} = \sqrt{\frac{1}{2}} \begin{pmatrix} 1 & 1 \\ -1 & 1 \end{pmatrix}, \tag{63}$$

then

$$\begin{aligned} |\Phi_0\rangle &= \tfrac{1}{2}(|00\rangle + |11\rangle + |01\rangle + |10\rangle) \\ &= \tfrac{1}{2}(|0\rangle + |1\rangle) \otimes (|0\rangle + |1\rangle) \end{aligned} \tag{64}$$

and

$$\begin{aligned} |\Phi_1\rangle &= \tfrac{1}{2}(|00\rangle - |11\rangle - |01\rangle + |10\rangle) \\ &= \tfrac{1}{2}(|0\rangle - |1\rangle) \otimes (|0\rangle - |1\rangle). \end{aligned} \tag{65}$$

Therefore, the entanglement of both $|\Phi_0\rangle$ and $|\Phi_1\rangle$ is zero. So the entanglement of this decomposition gives zero. Since you can't get less than zero, the entanglement of this mixed state is zero.

For a general density matrix,

$$\begin{aligned} |\Phi_\varsigma\rangle\langle\Phi_\varsigma| &= \frac{1}{q_\varsigma} \sum_{m,n=0}^{L-1} P_{\varsigma,m,n} |m\rangle\langle n| \\ &= \frac{1}{q_\varsigma} \sum_{\sigma,\varpi=0}^{\mathrm{rank}\{\hat{\rho}\}-1} U_{\varsigma\sigma} U^\dagger_{\varpi\varsigma} \sqrt{p_\sigma}\sqrt{p_\varpi} \\ &\quad \times \sum_{m,n=0}^{L-1} D^\dagger_{\sigma m} D_{n\varpi} |m\rangle\langle n|, \end{aligned} \tag{66}$$

where we have generalized the notation of Eqs. (56) and (57) so that $\boldsymbol{D}$ is a matrix of size $L \times L$ used to diagonalize the density matrix $\hat{\rho}$ and we have introduced the term $P_{\varsigma,m,n}$. According to the prescription in Eq. (49), the entanglement measure is applied to the pure state terms $|\Phi_\varsigma\rangle\langle\Phi_\varsigma|$. The BKOV entanglement measure consists of terms of the form [44]

$$[\mathrm{tr}\{|\Phi_\varsigma\rangle\langle\Phi_\varsigma|\boldsymbol{E}_\alpha\}]^2 = \frac{1}{q_\varsigma^2}\left[\mathrm{tr}\left\{\sum_{m,n=0}^{L-1} P_{\varsigma,m,n}|m\rangle\langle n|\boldsymbol{E}_\alpha\right\}\right]^2, \tag{67}$$

where the $\boldsymbol{E}_\alpha$ are Hermitian matrices that collectively form the basis for the Lie algebra (multiplied by $i = \sqrt{-1}$) required for the BKOV measure.

The BKOV entanglement of the decomposition is then of the form

$$\begin{aligned} &\mathcal{B}_{\mathrm{decomp}}(\boldsymbol{U}) \\ &\quad = 1 - \sum_{\alpha,\varsigma} \frac{1}{q_\varsigma}(\boldsymbol{U})\left[\mathrm{tr}\left\{\sum_{m,n=0}^{L-1} P_{\varsigma,m,n}(\boldsymbol{U})|m\rangle\langle n|\boldsymbol{E}_\alpha\right\}\right]^2. \end{aligned} \tag{68}$$

The $P_{\varsigma,m,n}$ terms are homogeneous functions of the matrix elements of $\boldsymbol{U}$ and $\boldsymbol{U}^\dagger$. These terms can then be viewed as homogeneous polynomials of degree two in $\mathbb{R}^{2K^2}$ but constrained to the compact subset $\mathrm{SU}(K) \subset \mathbb{C}^{K^2}$. The $P_{\varsigma,m,n}$ terms are squared, so we have a homogeneous polynomial of degree four in the numerator. The denominator is,

$$q_\varsigma = \sum_{\sigma=0}^{\mathrm{rank}\{\hat{\rho}\}-1} p_\sigma |U_{\varsigma\sigma}|^2, \tag{69}$$

which is a homogeneous polynomial of degree two. So, $1 - \mathcal{B}_{\mathrm{decomp}}$ is a ratio of homogeneous polynomials, of degree four in the numerator and of degree two in the denominator.

The only known bound on decompositions is that for a density matrix of $\mathrm{rank}\{\hat{\rho}\}$, decompositions from $\mathrm{SU}([\mathrm{rank}\{\hat{\rho}\}]^2)$ suffices for evaluating the convex roof [25,28]. For the density matrix $\hat{\rho}_s$ that we gave in Sec. IV, we find that this limit is much too large. Numerical calculation indicates that, as in the previous example, we can always choose $K = \mathrm{rank}\{\hat{\rho}_s\}$. Choosing $K > \mathrm{rank}\{\hat{\rho}_s\}$, that is, finer decompositions, is unnecessary for our model. If the rank of the density matrix is low, say 2 or 3, this makes the convex roof calculation tractable.

Knowing that we need only consider decompositions of the density matrix corresponding to unitary matrices of $\mathrm{SU}(K)$ with $K = \mathrm{rank}\{\hat{\rho}_s\}$, we still need to search all of $\mathrm{SU}(K)$. However, as we have just seen, the BKOV entanglement measure

is a ratio of two homogeneous polynomials. Furthermore, the denominator is never zero when restricted to SU(K). Since SU(K) is compact, our problem is to minimize such a function on a compact set. We can thus expect that the entanglement as a function of decompositions should be reasonably well behaved. So a search of SU(K) for the minimum BKOV entanglement can be quite coarse.

To search SU(K), we first parametrize the K^2-1 dimensional Lie group with a hypercube. The method of parametrization has been inductively worked out for arbitrary K in [52]. For SU(2) this parametrization is given by

$$\boldsymbol{U} = \exp(i\sigma_z\alpha_1)\exp(i\sigma_y\alpha_2)\exp(i\sigma_z\alpha_3), \tag{70}$$

where the σ's are the Pauli matrices, and the $0 \leqslant \alpha$'s $\leqslant 2\pi$ are the variables in the parametrization.

Likewise, using the same notation used in [52], we have that the parametrization for SU(3) is given by

$$\boldsymbol{U} = e^{i\lambda_3\alpha_1}e^{i\lambda_2\alpha_2}e^{i\lambda_3\alpha_3}e^{i\lambda_5\alpha_4}e^{i\lambda_3\alpha_5}e^{i\lambda_2\alpha_6}e^{i\lambda_3\alpha_7}e^{i\lambda_8\alpha_8}, \tag{71}$$

where

$$\lambda_3 = \begin{pmatrix} 1 & 0 & 0 \\ 0 & -1 & 0 \\ 0 & 0 & 0 \end{pmatrix}, \quad \lambda_8 = \begin{pmatrix} 1 & 0 & 0 \\ 0 & 1 & 0 \\ 0 & 0 & -2 \end{pmatrix}, \tag{72}$$

$$\lambda_2 = \begin{pmatrix} 0 & -i & 0 \\ i & 0 & 0 \\ 0 & 0 & 0 \end{pmatrix}, \quad \lambda_5 = \begin{pmatrix} 0 & 0 & -i \\ 0 & 0 & 0 \\ i & 0 & 0 \end{pmatrix} \tag{73}$$

are four matrices of the Lie algebra $\mathfrak{su}(3)$ and the $0 \leqslant \alpha$'s $\leqslant 2\pi$ are again the variables in the parametrization. The formulas get progressively longer for higher K, so we refer the reader to the source [52].

Next, we remark that examination of the formula for entanglement strongly suggests that the minimum over decompositions $\boldsymbol{U}$ should be quite broad and multidimensional. This implies that a very simple algorithm should suffice in finding the minimum. The algorithm we use is a much simpler version of the one given in [53]. First, we form an evenly spaced grid of 2^n points in the hypercube that parametrizes SU(K). It is usually sufficient to choose $n < K^2-1 =$ dimension of SU(K). So, for example, while 2^3 grid points would subdivide the parameter space of SU(2), which is three dimensional, into eight equal-size volumes, this level of refinement is unnecessary. A grid of 2^2 points dividing the parameter space into four volumes suffices for our algorithm. The grid points could be (0,0,0), (π,0,0), (0,π,0), and (π,π,0), with the understanding that 2π is identified with 0 in the parameter space given in [52].

In the gridding scheme we use in this article, the first K^2-2 coordinates take on the two possible values, 0 or π, along each axis α_i. The last coordinate has only one possible value, which is 0. If we are using decompostions from SU(3), then a grid with 2^7 points would have coordinates 0 or π along seven of the axes and the value 0 on the eighth axis. The reason for gridding up the parameter space to begin with is to avoid local minima and areas where the entanglement measure has no gradient. Since the BKOV entanglement measure is a ratio of homogeneous polynomials on a compact set, we do not expect many local extrema. In fact, we have found that for our model, alternative local minima show up only when the number of grid points for SU(K) are below $2^{\dim\{\mathrm{SU}(K)\}/2}$. So the calculation need not be very computer intensive.

In the next step of our algorithm, we calculate the entanglement of the decomposition at each grid point. At each grid point we then move 5° along each axis to determine if the entanglement function decreases. If it does not, the "ball" stops rolling. So, for example, a point in SU(3) has 16 possible directions corresponding to the positive and negative directions on the eight axes. Starting at the grid point, one moves incrementally in each direction to determine which axis gives the minimal entanglement. When that axis is determined, a new starting point is set along that axis and the comparison of all directions is repeated. When movement along the axes no longer decreases the entanglement we have the minimal entanglement associated to the original grid point.

Finally, we collect the minima calculated for each grid point. The minimum of this set we take to be our best approximation of the correct answer. More grid points, or a finer search at each grid point, will lead to finer approximations of the answer. Conversely, we find that alternative local minima do not show up until our step spacing gets as large as 30° or the number of grid points is smaller than $2^{\dim\{\mathrm{SU}(K)\}/2}$.

VII. RESULTS OF THE NUMERICAL CALCULATIONS

We now present our results of the numerical calculation of the CRE. In this section we will only consider the superradiant case where all the system oscillators are initially excited with the same phase so that $\bar{\mu} = \mu$ in Eq. (32). Our calculations of BKOV entanglement are all done with the following Lie algebra,

$$\mathfrak{g} = \bigoplus_{p=0}^{N-1} \mathfrak{su}(L_p), \tag{74}$$

where N is the number of parties on our system, $\mathfrak{su}(L_p)$ is the Lie algebra of $L_p \times L_p$ traceless anti-Hermitian matrices, and L_p is the dimension of the pth party.

In Fig. 1 we compare the CRE of the BKOV measure to Wootter's concurrence $\mathcal{C}$ [11] and the convex roof of the entanglement of formation $\mathcal{F}$. Recall that the convex roof of the entanglement of formation is related to the concurrence via the relations [10]

$$\mathcal{F}(\mathcal{C}) = h\left(\frac{1+\sqrt{1-\mathcal{C}^2}}{2}\right), \tag{75}$$

where

$$h(x) = -x\log_2(x) - (1-x)\log_2(1-x). \tag{76}$$

While all three measures give different results between zero and complete entanglement, they all demonstrate the same generic decay. The graphs also demonstrate the similarity between $\mathcal{F}$ and BKOV as bipartite measures. Of course, with increasing μ, the increasing steepness of the entanglement decay guarantees that all three measures converge in value. Plotted as well, for time comparison, is the function $e^{-2\gamma t}$, which gives the amplitude decay of the oscillator in Eq. (28). For large μ the decay is exponentially faster than the amplitude decay. This effect is due to dephasing of the Schrödinger

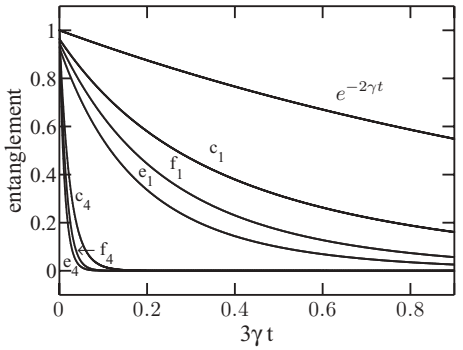

FIG. 1. Entanglement vs time ($0 \leqslant 3\gamma t \leqslant 0.9$), comparing three different measures, for a Schrödinger-cat state in a bipartite two-level Hilbert space. The entanglement of the density matrix in Eq. (29) is compared using three different measures for the case $M = N = 2$ and $\mathscr{S} = 0$. Graphs marked with the letter c denote the concurrence measure. Graphs marked with the letter f denote the entanglement of formation derived from the concurrence. Finally, graphs marked by the letter e denote our calculation of the convex roof of BKOV using SU(2) decompositions. The subscripts to the letters denote the cases of $\mu = 1$ and 4. The decay $e^{-2\gamma t}$ of the system oscillator amplitude is displayed as well for time comparison.

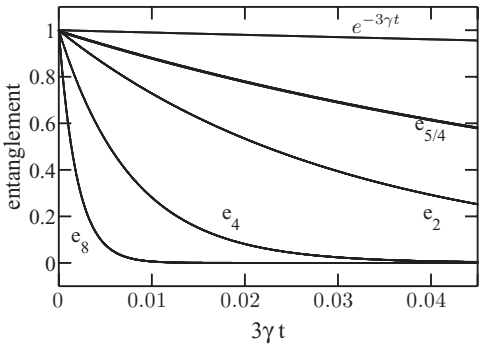

FIG. 2. Entanglement vs time ($0 \leqslant 3\gamma t \leqslant 0.045$), comparing three different measures, for a large-amplitude Schrödinger-cat state in a tripartite two-level Hilbert space. BKOV entanglement vs π-tangle vs 3-tangle for $\mu = \frac{5}{4}\,(e_{5/4}), 2\,(e_2), 4\,(e_4)$, and $8\,(e_8)$ in the case of $N = 3$ and $M = 2$. The calculation of BKOV is done using decompositions $\boldsymbol{U} \in \mathrm{SU}(2)$ because this is the approximate rank of $\hat{\rho}_s$. Note that the three measures overlap with a very slight difference noticeable for $\mu = 5/4$.

cat, where different time scales for dephasing and amplitude decay were first noted by [37,54]. In the context of bipartite discrete systems, this effect was again noted in the context of entanglement by [55]. Rapid mixing is the effect we expect from a bath and we see that for moderately large μ, this mixing leads to rapid decay of entanglement. On the other hand, for small μ, the decay in entanglement is of the same order of magnitude as the amplitude decay. The mixing of the state by the bath has a less dramatic effect on the entanglement.

The preceding observations suggest that large-amplitude entangled Schrödinger-cat states have quite different dynamical evolution than small-amplitude Schrödinger-cat states. By large-amplitude Schrödinger-cat state we mean a superposition of coherent states where the coherent state amplitude is much larger than one, and an entangled cat is an entangled state. A small-amplitude Schrödinger-cat state is then a superposition of coherent states where the coherent state amplitude is less than, or close to, one. Then we observe that the evolution of large-amplitude entangled Schrödinger-cat states takes place on a different time scale than for small-amplitude Schrödinger-cat states. The former has a time scale governed by the decay of correlations in the reservoir while the latter has time scale governed by the decay of the system oscillator amplitudes.

Next, we numerically calculate the CRE for a tripartite system, that is, $N = 3$ in Eq. (29). We first consider the case where $M = 2$, so that in our circular basis [Eq. (45)], the number of levels in each of the three parties is two. In Figs. 2 and 3 we plot the CRE of BKOV vs the 3-tangle [19] and the π-tangle [56]. For values of $\mu > 1$, we see from Fig. 2 that the three measures coincide for our model, with very slight separation (BKOV on top, 3-tangle at bottom) when $\mu = \frac{5}{4}$. This confirms our statement in the Introduction that our states are GHZ-like, as the 3-tangle only measures GHZ-type entanglement [19,57]. When $\mu \leqslant 1$, the three measures disagree, as seen in Fig. 3. The π-tangle and BKOV are similar but differ increasingly from the 3-tangle as μ gets smaller. The conclusion is that for small μ our states are not GHZ-like.

Next, we consider the case where $M = 3$, so that in our circular basis [Eq. (45)], the number of levels in each of the three parties is three. In Fig. 4 we plot our calculation of the CRE of BKOV using decompositions from SU(2) when the rank of the reduced density matrix is 2 and SU(3) when the rank is 3. The rank was determined by considering only eigenvalues above a cutoff of 10^{-4}. Since the trace must be one, this guarantees that the eigenvalues discarded are several orders of magnitude smaller than the largest eigenvalue. From the figure we see that for values of $\mu \geqslant 2$ the decay of entanglement is much more rapid, in fact exponentially so, compared to the oscillator amplitude decay rate $e^{-3\gamma t}$.

We can do this calculation because the rank of the density matrix in this case can be approximated as 2 or 3. Furthermore, only decompositions through SU(2) or SU(3), depending on the rank, are necessary in our case. Higher-order unitary matrices offer no significant improvement.

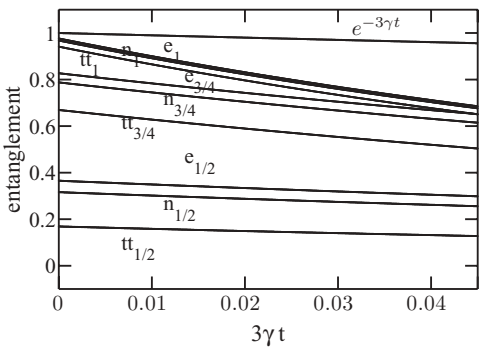

FIG. 3. Entanglement vs time ($0 \leqslant 3\gamma t \leqslant 0.045$), comparing three different measures, for a small-amplitude Schrödinger-cat state in a tripartite two-level Hilbert space. BKOV entanglement (e) vs π-tangle (n) vs 3-tangle (tt) for $\mu = \frac{1}{2}, \frac{3}{4}$, and 1 (denoted as subscripts on e, n, and tt) in the case of $N = 3$ and $M = 2$. The calculation of BKOV is done using decompositions $\boldsymbol{U} \in \mathrm{SU}(2)$ because this is the approximate rank of $\hat{\rho}_s$.

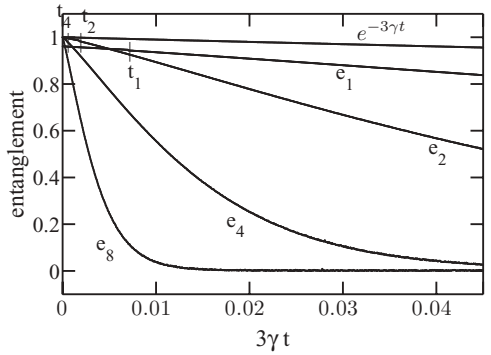

FIG. 4. Entanglement vs time ($0 \leqslant 3\gamma t \leqslant 0.045$) for a large-amplitude Schrödinger-cat state in a tripartite three-level Hilbert space. BKOV entanglement for $\mu = 1$ (e_1), 2 (e_2), 4 (e_4), and 8 (e_8) in the case of $N = M = 3$. The calculation is done using decompositions $\boldsymbol{U} \in \mathrm{SU}(K)$, where $K =$ rank of $\hat{\rho}_S$ for the case of $N = M = 3$. The rank of the reduced density matrix is 1 at $t = 0$ and then changes instantaneously to 2 on the time scale used in the plot. The times marked t_4, t_2, and t_1 denote the points where the rank of $\hat{\rho}_S$ changes from 2 to 3 for the cases $\mu = 4$, 2, and 1, respectively. In the case of $\mu = 8$, the rank of the reduced density matrix changes from 1 to 3 almost instantaneously on the time scale used in the plot.

Figure 5 illustrates this point. The fine curves in the figure are calculated using decompositions from $SU(K) = \mathrm{rank}\{\hat{\rho}_S\}$. In this case, for $t > 0$, the rank is 2 or 3 as shown in Fig. 4 . The large coarse points represent the calculation of entanglement using the finer decomposition of SU(4). One can see that there is no significant decrease in the entanglement calculated with the finer decomposition.

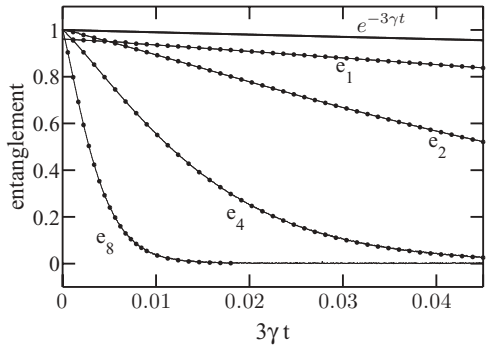

FIG. 5. The effect on CRE using finer decompositions in the tripartite three-level case. Short-time ($0 \leqslant 3\gamma t \leqslant 0.045$) graph of BKOV entanglement for the case of $N = M = 3$, where we compare two different decompositions for the cases $\mu = 1$, 4, and 8. Graphs of the two decompositions are superimposed. The coarser decomposition gives rise to the continuous-looking curves, which are calculated using $\boldsymbol{U} \in \mathrm{SU}(K)$, where $K = \mathrm{rank}\{\hat{\rho}_S\}$, For $\mu = 4$ and 10 and $t > 0$, the the rank of the density matrix is 3 and we use SU(3) for the decomposition. When $\mu = 2$ and $t > 0$, the rank starts out at 2 and then becomes 3. So we first calculate entanglement in this case using decompositions only from SU(2) when the rank is 2 and then from SU(3) when the rank becomes 3. The finer decomposition is marked by the large discrete points. The entanglement calculation at each time point is done using $\mathrm{SU}(K) = \mathrm{SU}(4)$. As is evident from the graphs, there is no significant improvement in going to finer decompositions. So it is sufficient to check the convex roof with $K = \mathrm{rank}\{\hat{\rho}_B\}$.

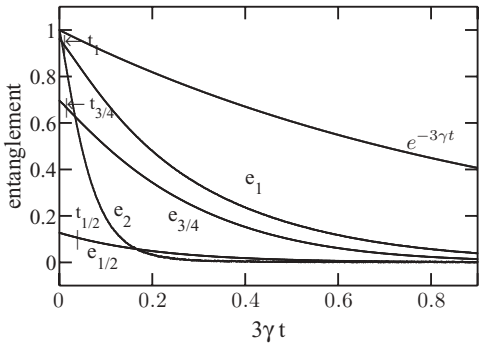

FIG. 6. Entanglement vs time ($0 \leqslant 3\gamma t \leqslant 0.9$) for a small-amplitude Schrödinger-cat state in a tripartite three-level Hilbert space. Entanglement for $\mu = 1/2$ ($e_{1/2}$), 3/4 ($e_{3/4}$), 1 (e_1), and 2 (e_2) in the case of $N = M = 3$. The calculation was done with $\boldsymbol{U} \in \mathrm{SU}(K)$, where $K =$ rank of $\hat{\rho}_S$. The rank of the reduced density matrix is 1 at $t = 0$ and then changes instantaneously to 2 on the time scale used in the plot. The times marked t_1, $t_{3/4}$, and $t_{1/2}$ denote the points where the rank of $\hat{\rho}_S$ changes from 2 to 3 for the cases $\mu = 1$, 3/4, and 1/2, respectively. In the case of $\mu = 2$, the rank of the reduced density matrix changes from 1 to 3 almost instantaneously on the time scale used in the plot. The subscripts denote the value of μ. Note that when $\mu \leqslant 1$, the initial entanglement is no longer equal to one.

For small μ, that is $\mu \leqslant 1$, we see, from Fig. 6, that the entanglement decay rate is significantly slower then the super-exponential decay exhibited in the high-μ case. Now the decay of entanglement is of the same order as the amplitude decay rate $e^{-3\gamma t}$. In addition, for $\mu \leqslant 1$, the initial entanglement is no longer complete, and the initial value of entanglement decreases rapidly with decreasing μ. To summarize, if we start with a high amount of initial entanglement, the decay of entanglement is extremely rapid. If we start with very little entanglement, the decay of entanglement is much slower.

In Figs. 7 and 8 we compare the decay of entanglement using the convex roof of BKOV to the decay of the real part of the off diagonal bath inner product (ODBIP) from Eq. (36)

$$\mathrm{Re}\left\{\prod_B \langle\beta_{\sigma=1,B}|\beta_{\varsigma=2,B}\rangle\right\} = \exp\{-|\mu|^2[1-\cos(-2\pi(1-2)/3)](1-e^{-2\times 3\gamma t})\}. \tag{77}$$

From the two figures we can identify several features about the decay of entanglement for $\mu \geqslant 2$:

(i) The decay rate of the ODBIP term and the decay rate of the entanglement coincide for a time $t \in [0, t_1(\mu)]$.

(ii) The time $t_2(\mu)$ that it takes for the ODBIP term to reach its exponential knee (defined as the point where the slope is -1), coincides with the time it takes for the BKOV entanglement to decay to zero.

(iii) The average rate of decay of the ODBIP term in the time interval $t \in [0, t_2(\mu)]$ is much much greater than -3γ.

(iv) For the time $t \in [0, t_2(\mu)]$ the average decay rate of BKOV entanglement is greater than that for the ODBIP term. In fact, the entanglement decay rate is nearly constant for approximately 2/3 of the decay.

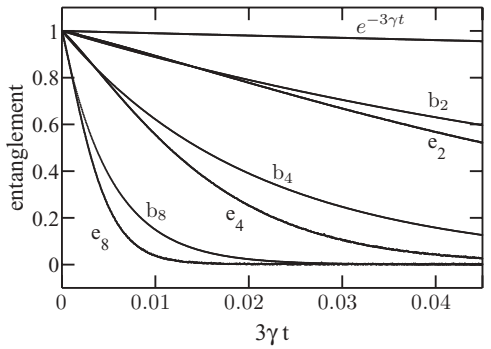

FIG. 7. Comparison of time entanglement ($0 \leqslant 3\gamma t \leqslant 0.045$) of a large-amplitude Schrödinger-cat state with reservoir correlation decay in a tripartite three-level Hilbert space using BKOV convex roof. Entanglement is computed using decompositions $\boldsymbol{U} \in \mathrm{SU}(K)$, where $K =$ rank of $\hat{\rho}_S$ for the case of $N = M = 3$. Plotted next to each entanglement graph, e_k, is a plot of the off-diagonal bath product term, b_k, given by Eq. (77). The subscripts denote the value of μ. Note that the off-diagonal bath decay rate completely determines the initial entanglement decay rate for the given μ. After a fixed time the BKOV decay rate is nearly the same as its initial value. On the other hand, the bath decay rate, which decays superexponentially, becomes exponentially smaller than the BKOV decay rate.

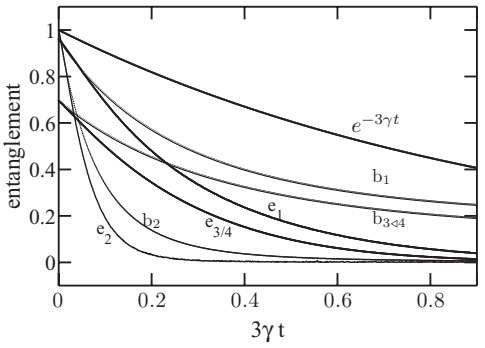

FIG. 8. Comparison of time entanglement ($0 \leqslant 3\gamma t \leqslant 0.9$) of small-amplitude Schrödinger-cat states with reservoir correlation decay in a tripartite three-level Hilbert space using BKOV convex roof. Entanglement is computed using decompositions $\boldsymbol{U} \in \mathrm{SU}(K)$, where $K =$ rank of $\hat{\rho}_S$ for the case of $N = M = 3$. Plotted next to each entanglement graph is the decay of the bath coherence product of Eq. (77). Note that when $\mu \leqslant 1$, the initial entanglement is no longer equal to one. To compare rates to the bath decoherence, we have translated Eq. (77) to the value of the entanglement at time $t = 0$. b_2, b_1, and $\mathrm{b}_{3/4}$ represent the off-diagonal bath inner-product decay for the cases $\mu = 2$, 1, and $3/4$, respectively. As μ decreases below 1, the initial decay rate for BKOV entanglement is no longer the same as the decay rate of bath decoherence. The decay rate of entanglement is now determined by the oscillator amplitude decay rate.

These observations suggest that the off-diagonal bath product term in Eq. (77) plays a critical role in the extremely fast decay of entanglement for large μ. For $\mu \geqslant 2$, the ODBIP term limits to $e^{-(1+\sqrt{3}/2)|\mu|^2} \sim 0$ as $t \to \infty$. The decay of the ODBIP term is thus complete. The exponential knee of the ODBIP term is therefore close to zero as well, and the time to reach the knee is much shorter than the oscillator amplitude decay time. The decay time to the exponential knee of the entanglement curve is even faster, since the decay rate is nearly constant and is set by the initial decay rate of the ODBIP term.

When $\mu \leqslant 1$, the limiting exponential, $e^{-(1+\sqrt{3}/2)|\mu|^2}$, in the ODBIP term is non-negligible compared to one. So the total amount of ODBIP decay is limited, and its effect on entanglement decay is therefore limited as well. Furthermore, the time to reach this plateau is about 20 times slower than for $\mu = 8$. As a result, the decay rate for $\mu \leqslant 1$, as seen in Fig. 8, is of the same magnitude as the oscillator amplitude decay rate, that is, -3γ. Consequently the amplitude decay becomes a determining factor in the entanglement decay rate for small μ. Since the decoherence of the bath and oscillator amplitude decay are much slower processes for small μ, the decay of entanglement for small μ is also much slower. A way to summarize these results is to state that the evolution of large-amplitude entangled Schrödinger-cat states takes place on a different time scale than the evolution of small-amplitude entangled Schrödinger-cat states. The time evolution of the latter is comparable to the system amplitude decay rate.

VIII. CONCLUSION

We have calculated directly the time-dependent entanglement via the CRE of a collection of entangled harmonic oscillators interacting with a zero-temperature bath. The technique we employ should be generally useful for multipartite multilevel systems with density matrices of low rank. Our calculations illuminate the role of initial conditions and bath dephasing on the evolution of the initially entangled system. We show that the time scale of the evolution of the entanglement is dependent strongly on the level of excitation of the initial state. Large-amplitude Schrödinger-cat states decohere much more rapidly than small-amplitude Schrödinger-cat states.

[1] D. Braun, P. A. Braun, and F. Haake, Opt. Commun. **179**, 411 (2000).
[2] K. M. Fonseca-Romero, S. G. Mokarzel, and M. C. Nemes, e-print arXiv:quant-ph/0202031v1.
[3] Z. Ficek and S. Swain, *Quantum Interference and Coherence: Theory and Experiments*, Springer Series in Optical Sciences, 1st ed. (Springer, New York, 2004).
[4] W. Dür and H. J. Briegel, Phys. Rev. Lett. **92**, 180403 (2004).
[5] L. Viola, E. M. Fortunato, M. A. Pravia, E. Knill, R. Laflamme, and D. G. Cory, Science **293**, 2059 (2001).
[6] J. B. Altepeter, P. G. Hadley, S. M. Wendelken, A. J. Berglund, and P. G. Kwiat, Phys. Rev. Lett. **92**, 147901 (2004).
[7] P. G. Kwiat, A. J. Berglund, J. B. Altepeter, and A. G. White, Science **290**, 498 (2000).
[8] I. Bengtsson and K. Życzkowski, *Geometry of Quantum States: An Introduction to Quantum Entanglement*, 1st ed. (Cambridge University Press, Cambridge, UK, 2006).
[9] M. J. Donald, M. Horodecki, and O. Rudolph, J. Math. Phys. **43**, 4252 (2002).
[10] S. Hill and W. K. Wootters, Phys. Rev. Lett. **78**, 5022 (1997).

[11] W. K. Wootters, Phys. Rev. Lett. **80**, 2245 (1998).
[12] J. Schlienz and G. Mahler, Phys. Lett. A **224**, 39 (1996).
[13] N. Linden, S. Popescu, and A. Sudbery, Phys. Rev. Lett. **83**, 243 (1999).
[14] A. Acin, A. Andrianov, L. Costa, E. Jane, J. I. Latorre, and R. Tarrach, Phys. Rev. Lett. **85**, 1560 (2000).
[15] D. A. Meyer and N. Wallach, in *Mathematics of Quantum Computation*, Computational Mathematics, 1st ed., edited by R. K. Brylinski and G. Chen (Chapman and Hall/CRC Press, Boca Raton, FL, 2002), pp. 77–98.
[16] N. Wallach, Acta Appl. Math. **86**, 203 (2005).
[17] S. N. Walck, J. K. Glasbrenner, M. H. Lochman, and S. A. Hilbert, Phys. Rev. A **72**, 052324 (2005).
[18] A. Uhlmann, Phys. Rev. A **62**, 032307 (2000).
[19] V. Coffman, J. Kundu, and W. K. Wootters, Phys. Rev. A **61**, 052306 (2000).
[20] A. Wong and N. Christensen, Phys. Rev. A **63**, 044301 (2001).
[21] P. Rungta, V. Bužek, C. M. Caves, M. Hillery, and G. J. Milburn, Phys. Rev. A **64**, 042315 (2001).
[22] C. S. Yu and H. S. Song, Phys. Rev. A **71**, 042331 (2005).
[23] D. Li, X. Li, H. Huang, and X. Li, J. Math. Phys. **50**, 012104 (2009).
[24] L. P. Hughston, R. Jozsa, and W. K. Wootters, Phys. Lett. A **183**, 14 (1993).
[25] A. Uhlmann, Open Sys. Inf. Dyn. **5**, 209 (1998).
[26] S. Lee, D. P. Chi, S. D. Oh, and J. Kim, Phys. Rev. A **68**, 062304 (2003).
[27] F. Mintert, M. Kus, and A. Buchleitner, Phys. Rev. Lett. **92**, 167902 (2004).
[28] F. Mintert, A. R. Carvalho, M. Kus, and A. Buchleitner, Phys. Rep. **415**, 207 (2005).
[29] F. Mintert, M. Kus, and A. Buchleitner, Phys. Rev. Lett. **95**, 260502 (2005).
[30] C. S. Yu, X. X. Yi, and H. S. Song, Phys. Rev. A **78**, 062330 (2008).
[31] J. S. Kim, A. Das, and B. C. Sanders, Phys. Rev. A **79**, 012329 (2009).
[32] R. Lohmayer, A. Osterloh, J. Siewert, and A. Uhlmann, Phys. Rev. Lett. **97**, 260502 (2006).
[33] C. Eltschka, A. Osterloh, J. Siewert, and A. Uhlmann, New J. Phys. **10**, 043014 (2008).
[34] E. Jung, M. R. Hwang, D. K. Park, and J. W. Son, Phys. Rev. A **79**, 024306 (2009).
[35] I. A. Pedrosa and B. Baseia, Phys. Rev. D **30**, 765 (1984).
[36] C. M. Savage and D. F. Walls, Phys. Rev. A **32**, 2316 (1985).
[37] D. F. Walls and G. J. Milburn, Phys. Rev. A **31**, 2403 (1985).
[38] J. P. Paz, S. Habib, and W. H. Zurek, Phys. Rev. D **47**, 488 (1993).
[39] D. Braun, Phys. Rev. Lett. **89**, 277901 (2002).
[40] F. Benatti and R. Floreanini, J. Phys. A **39**, 2689 (2006).
[41] M. A. Landau and C. R. Stroud Jr., Phys. Rev. A **77**, 062104 (2008).
[42] H. Barnum, E. Knill, G. Ortiz, and L. Viola, Phys. Rev. A **68**, 032308 (2003).
[43] H. Barnum, E. Knill, G. Ortiz, R. Somma, and L. Viola, Phys. Rev. Lett. **92**, 107902 (2004).
[44] R. Somma, G. Ortiz, H. Barnum, E. Knill, and L. Viola, Phys. Rev. A **70**, 042311 (2004).
[45] L. Viola, H. Barnum, E. Knill, G. Ortiz, and R. Somma, e-print arXiv:quant-ph/0403044v1.
[46] D. A. Meyer and N. R. Wallach, J. Math. Phys. **43**, 4273 (2002).
[47] P. Love, A. M. van Brink, A. Y. Smirnov, M. H. S. Amin, M. Grajcar, E. Il'ichev, A. Izmalkov, and A. M. Zagoskin, Quantum Inf. Process. **6**, 187 (2007).
[48] Limited superradiant damping of small samples R. Friedberg (Columbia Univ., NY, USA); S. R. Hartmann and J. T. Manassah, Phys. Lett. A **40A**, 365 (1972).
[49] H. J. Carmichael, *Statistical Methods in Quantum Optics 1: Master Equations and Fokker-Planck Equations*, Theoretical and Mathematical Physics, vol. 1 (Springer, New York, 1998).
[50] R. Dicke, Phys. Rev. **93**, 99 (1954).
[51] M. A. Schlosshauer, *Decoherence and the Quantum-to-Classical Transition*, The Frontiers Collection (Springer-Verlag, Berlin, 2007).
[52] T. Tilma and E. Sudarshan, J. Phys. A **35**, 10467 (2002).
[53] K. Audenaert, F. Verstraete, and B. DeMoor, Phys. Rev. A **64**, 052304 (2001).
[54] W. G. Unruh and W. H. Zurek, Phys. Rev. D **40**, 1071 (1989).
[55] T. Yu and J. H. Eberly, Phys. Rev. B **66**, 193306 (2002).
[56] Y. C. Ou and H. Fan, Phys. Rev. A **75**, 062308 (2007).
[57] E. Jung, D. K. Park, and J. W. Son, Phys. Rev. A **80**, 010301(R) (2009).